

Superconducting Penetration Depth Through a Van Hove Singularity: Sr_2RuO_4 Under Uniaxial Stress

Eli Mueller,^{1,2} Yusuke Iguchi,^{1,3} Fabian Jerzembeck,⁴ Jorge O. Rodriguez,⁵ Marisa Romanelli,⁵ Edgar Abarca-Morales,⁴ Anastasios Markou,^{4,6} Naoki Kikugawa,⁷ Dmitry A. Sokolov,⁴ Gwansuk Oh,^{8,9} Clifford W. Hicks,^{4,10} Andrew P. Mackenzie,^{4,11} Yoshiteru Maeno,^{8,12} Vidya Madhavan,⁵ and Kathryn A. Moler^{1,2,3}

¹Stanford Institute for Materials and Energy Sciences, SLAC National Accelerator Laboratory, 2575 Sand Hill Road, Menlo Park, California 94025, USA

²Department of Physics, Stanford University, Stanford, California 94305, USA

³Geballe Laboratory for Advanced Materials, Stanford University, Stanford, California 94305, USA

⁴Max Planck Institute for the Chemical Physics of Solids, Nöthnitzer Straße 40, Dresden 01187, Germany

⁵Department of Physics, University of Illinois, Urbana, Illinois 61801, USA

⁶Department of Physics, University of Ioannina, 45110 Ioannina, Greece

⁷National Institute for Materials Science, Tsukuba, Ibaraki 305-0003, Japan

⁸Department of Physics, Graduate School of Science, Kyoto University, Kyoto 606-8502, Japan

⁹Department of Physics, Pohang University of Science and Technology (POSTECH), Pohang 790-784, Republic of Korea

¹⁰School of Physics and Astronomy, University of Birmingham, Birmingham B15 2TT, United Kingdom

¹¹Scottish Universities Physics Alliance, School of Physics and Astronomy,

University of St. Andrews, St. Andrews KY16 9SS, United Kingdom

¹²Toyota Riken - Kyoto University Research Center (TRiKUC), Kyoto University, Kyoto 606-8501, Japan

In the unconventional superconductor Sr_2RuO_4 , uniaxial stress along the [100] direction tunes the Fermi level through a Van Hove singularity (VHS) in the density of states, causing a strong enhancement of the superconducting critical temperature T_c . Here, we report measurements of the London penetration depth λ as this tuning is performed. We find that the zero-temperature superfluid density, here defined as $\lambda(0)^{-2}$, increases by $\sim 15\%$, with a peak that coincides with the peak in T_c . We also find that the low temperature form of $\lambda(T)$ is quadratic over the entire strain range. Using scanning tunneling microscopy, we find that the gap increases from $\Delta_0 \approx 350 \mu\text{eV}$ in unstressed Sr_2RuO_4 to $\Delta_0 \approx 600 \mu\text{eV}$ in a sample strained to near the peak in T_c . With a nodal order parameter, an increase in the superconducting gap could bring about an increase in the superfluid density through reduced sensitivity to defects and through reduced non-local effects in the Meissner screening. Our data indicate that tuning to the VHS increases the gap throughout the Brillouin zone, and that non-local effects are likely more important than reduced scattering.

Strontium ruthenate (Sr_2RuO_4) is a highly studied system in the field of unconventional superconductivity [1–8]. The metallic normal state from which superconductivity condenses is one of the simplest and best understood among unconventional superconductors [9], but after nearly three decades of strenuous effort, a complete understanding of the superconducting order parameter remains elusive.

The low-temperature behavior of the London penetration depth $\lambda(T)$ provides information on the existence of nodes in the superconducting gap $\Delta(k)$. The majority of experimental evidence suggests the presence of line nodes [10–15]. In the limit of large $\kappa = \lambda/\xi$, where λ and ξ are the penetration depth and coherence length respectively, it is well-known that an order parameter with line nodes yields a T -linear dependence in the low-temperature form of $\lambda(T)$ for clean samples, and a T^2 dependence in the presence of strong impurity scattering [16]. Measurements of $\lambda(T)$ in Sr_2RuO_4 have repeatedly shown a T^2 form [17–19]. However, it would be odd for the effects of impurity scattering to be strong in Sr_2RuO_4 because it is one of the cleanest correlated electron materials known, with the best available samples having a mean free path l exceeding $1 \mu\text{m}$ [20]. Alternatively, it was suggested in Ref. [17] that a $\lambda(T) \sim T^2$ dependence may be a result of non-local electrodynamic effects [21] because the superconductivity in Sr_2RuO_4 is only marginally in the local limit with $\kappa \approx 2.9$ at low temperature [17].

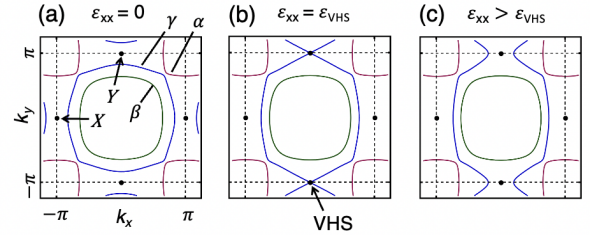


FIG. 1. Quasi-two-dimensional Fermi surface calculations of Sr_2RuO_4 under representative ϵ_{xx} strains [22]. (a) Fermi surface under zero strain, showing the two electron-like bands γ and β and the hole-like band α . Points labeled X and Y indicate high-symmetry points. (b) Fermi surface with the system strain-tuned to the Lifshitz transition. The VHS occurs on the γ band at the Y points. (c) Fermi surface for the system strained beyond the Lifshitz transition.

The advent of strain-tuning presents a new frontier for studying $\lambda(T)$. Uniaxial stress along the [100] direction drives the γ Fermi surface sheet through a Lifshitz transition (see Fig. 1 and Ref. [23]) and an associated Van Hove singularity (VHS) in the Fermi level density of states. In addition, the superconducting critical temperature T_c undergoes a dramatic enhancement from an unstressed value of $T_{c0} = 1.5 \text{ K}$ to a peak of 3.5 K [22, 24] at the VHS which is accompanied by a 20-fold increase in the out-of-plane critical field H_{c2} [22, 25].

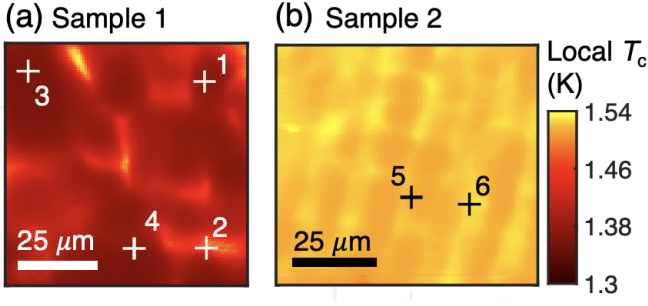


FIG. 2. Local T_c maps of (a) sample 1 and (b) sample 2. Markers indicate the positions at which the temperature and strain dependence of the penetration depth was measured.

In a weak-coupling picture, the enhanced superconductivity under strain is most intuitively explained by the increased density of states around the VHS [22, 26].

There are a few possible hypotheses for how the $T \rightarrow 0$ superfluid density $\lambda(0)^{-2}$ might change as the Lifshitz transition is traversed. Theoretical work [27] suggests that the quasiparticle mass renormalization on the γ sheet is a consequence of the proximity of the Fermi level to the VHS. Tuning to the VHS could cause a further increase in the effective mass m^* , thereby decreasing the superfluid density through the relation $\lambda^{-2} = 4\pi n_s e^2 / m^* c^2$, where n_s is the number density of superconducting electrons. Alternatively, an increase in the superconducting gap Δ_0 could reduce the effects of impurities and of non-locality in the Meissner screening, leading to an increase in the superfluid density. If the coherence length is strongly reduced by tuning to the Lifshitz transition, then it is also possible that the T^2 form of $\lambda(T) - \lambda(0)$ in unstressed Sr_2RuO_4 would become T -linear. We note that a subset of the present authors previously reported scanning superconducting quantum interference device (SQUID) measurements of the penetration depth on uniaxially stressed Sr_2RuO_4 [28]. In those measurements, the focus was to test for an anomaly in the superfluid density associated with a transition below T_c [29] and the maximum applied strain ϵ was well below the Lifshitz transition. In this letter, we report scanning SQUID measurements of the strain- and temperature-dependent changes of the penetration depth $\lambda(\epsilon, T) - \lambda(0, 0)$ in Sr_2RuO_4 across the Lifshitz transition. To aid interpretation of these data, we also report measurements by scanning tunneling microscopy (STM) of Δ_0 on Sr_2RuO_4 strained to near the Lifshitz transition.

The main components of our SQUID susceptometers [30] include a flux-sensitive pickup loop with an inner radius r_{PL} of $1 \mu\text{m}$ and a concentric field coil with an inner radius r_{FC} of $2.5 \mu\text{m}$. A low-frequency (893 Hz) alternating current is applied to the field coil, which generates a local field that couples to the SQUID pickup loop. Near a superconducting sample, the Meissner response screens the field from the field coil and reduces the mutual inductance M of the pickup-loop/field-coil pair, which we measure in units of Φ_0/A , where $\Phi_0 = h/2e$ is the flux quantum. Recording M as a function of temperature allows us to measure the local T_c by measuring the onset of diamagnetism ($M < 0$). In the regime where the penetration

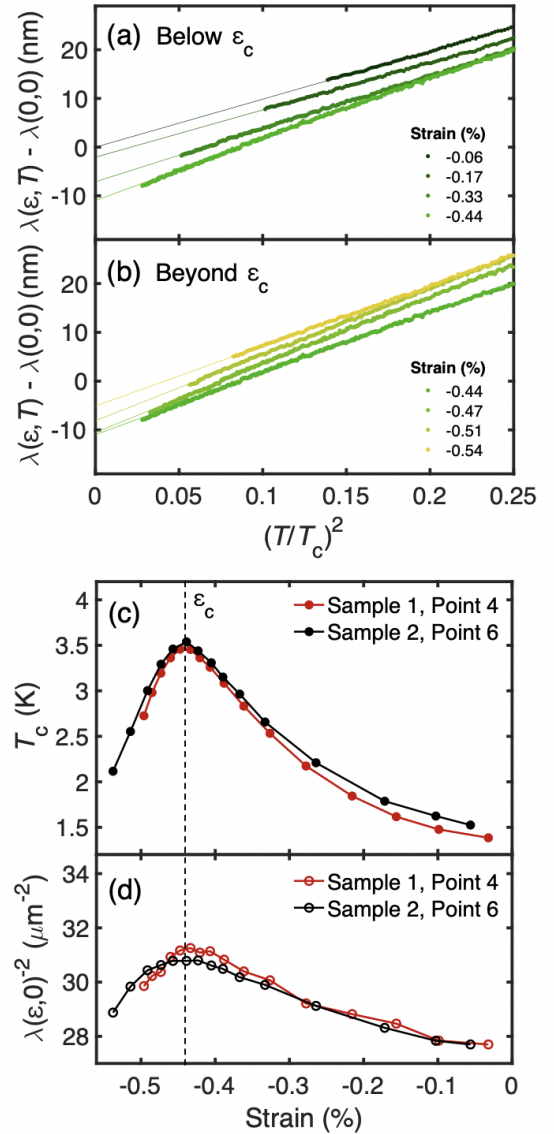


FIG. 3. (a) and (b) Temperature and strain dependence of the change in penetration depth $\lambda(\epsilon, T) - \lambda(0, 0)$ for strains (a) less than ϵ_c and (b) greater than ϵ_c for sample 2. Solid lines are T^2 fits to the data. We take $\lambda(0, 0)$ to be the $T = 0$ K intercept of a $\lambda(\epsilon, T) \sim T^2$ fit to the -0.06% strain dataset. (c) Strain dependence of local T_c measured on sample 1 (red) and 2 (black). (d) Strain dependence of the zero-temperature superfluid density $\lambda(\epsilon, 0)^{-2}$ for sample 1 (red) and sample 2 (black). For each dataset, the zero-temperature superfluid density at the minimum strain is set to $\lambda^{-2} = 27.7 \mu\text{m}^{-2}$ ($\lambda = 190 \text{ nm}$ [17]) and we estimate changes in $\lambda(\epsilon, 0)^{-2}$ by extrapolating the T^2 fits from (a) and (b) to $T = 0$ K.

depth is smaller than r_{FC} and the height of the field coil from the sample surface z_0 , the measured M can be used to estimate the quantity $\lambda(\epsilon, T) + z_0$ [31]. In our measurement, we fix z_0 by bringing the SQUID sensor into light mechanical contact with the sample surface to prevent drift of the SQUID so that changes in M are due to changes in $\lambda(\epsilon, T)$.

For the penetration depth measurements, *in situ* tunable strain was applied using a piezoelectric-driven device similar

to that described in previous reports [32, 33]. The device contains a capacitive sensor of applied displacement; to convert to strain, we set the strain to be zero at the minimum in T_c and to $\epsilon_c = -0.44\%$ at the peak in T_c [34]. To check reproducibility, we measured two samples cut from separate batches into bars ≈ 2 mm in length. Maps of local T_c were obtained near zero strain by taking spatial scans of M at a series of temperatures near the bulk T_c [35]. Sample 1 [Fig. 2(a)] shows a lower overall T_c of 1.36–1.4 K with a few small pockets of local T_c values as high as 1.5 K. Sample 2 [Fig. 2(b)] is more homogeneous and shows higher overall T_c values of 1.51–1.54 K. The apparent stripe pattern in the local T_c map of sample 2 is most likely due to periodic changes in the solidification condition during sample growth [36][37].

Figures 3(a) and (b), show the temperature and strain dependence of the change in penetration depth $\lambda(\epsilon, T) - \lambda(0, 0)$ plotted against $(T/T_c)^2$. For fixed T/T_c , the curves show a clear reduction in penetration depth with increasing strain below ϵ_c [Fig. 3(a)] and a subsequent increase in penetration depth for strains beyond ϵ_c [Fig. 3(b)]. The T^2 fits (solid lines) agree well with the data for $T < 0.5T_c$ over the entire strain range.

In Fig. 3(c), the T_c at two selected points is plotted against applied strain. The local T_c for each value of strain was determined from $M(T)$ by the temperature at which the maximum in dM/dT occurs [35]. The T_c versus strain curves for sample 1 and sample 2 approximately track each other; however, the difference between T_c of the two samples shrinks as T_c increases, consistent with the general expectation that higher T_c corresponds to reduced sensitivity to defect scattering. Figure 3(d) shows the strain dependence of the zero-temperature superfluid density $\lambda(\epsilon, 0)^{-2}$. Under increasing compression, $\lambda(\epsilon, 0)^{-2}$ increases monotonically up to ϵ_c , where it reaches an approximately 15% enhancement, then decreases for strains beyond ϵ_c .

For the STM measurements, due to the restricted sample space, strain was applied using a differential thermal expansion cell as in Ref. [23]. We estimate that the applied strain in the sample was $0.4 \pm 0.1\%$ using digital image correlation of the sample platform at low temperature; additional details are given in Ref. [35]. Data from the STM measurements are shown in Fig. 4. As in previous works [38–42], we do not observe a superconducting gap on the top strontium oxide (SrO) surface, possibly because of the surface reconstruction[43–45]. However, we do observe a superconducting gap inside several nanometer-scale trenches, most probably created when the sample was cleaved. In these trenches both the surface SrO layer and the RuO₂ layer directly below it are removed, thereby exposing the lower SrO layer which provides a window into the bulk properties [see Fig. 4(a)].

Figures 4(b) and (c) show typical topographies as well as spectroscopic linecuts [Fig. 4(d) and Fig. 4(e)] in these trenches in an unstrained and strained sample, respectively. In the unstrained sample [Fig. 4(d)], the spectra inside the trench show a well-defined gap with $2\Delta_0$ equal to approximately $700 \mu\text{V}$, as denoted by the dashed lines marking the position of the coherence peaks. We note that this value of $2\Delta_0$ is consistent with previous measurements on unstrained

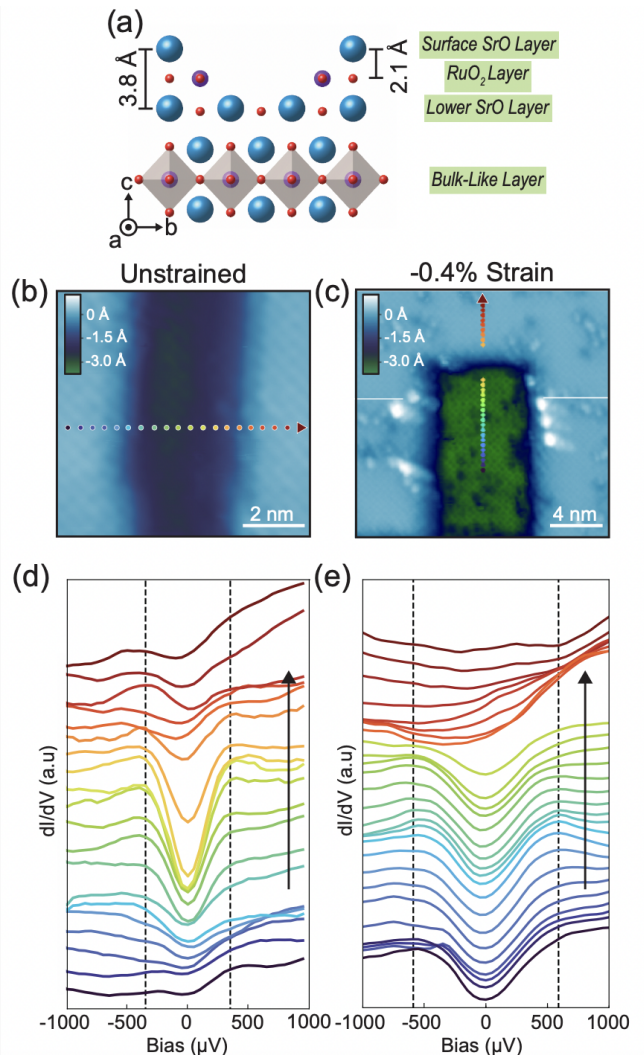


FIG. 4. Superconducting gap under the surface SrO layer in Sr₂RuO₄. (a) Schematic diagram of the crystal structure of Sr₂RuO₄ showing subsurface layers (b) Topographic image of a defect (dark blue area) on an unstrained sample exposing the RuO₂ layer at a depth of $\approx 2.1 \text{ \AA}$ (c) Topographic image of a defect (green area) on a strained sample exposing the lower SrO layer at a depth of $\approx 3.4 \text{ \AA}$. See Ref. [35] for details for determining the depth of the cleavage defects. The topographic depth indicated by the colorbar is measured relative to the surface SrO layer (light blue area) (d) Waterfall plot of dI/dV spectroscopy data measured at the points indicated in (b). (e) Waterfall plot of dI/dV spectroscopy data measured at the points indicated in (c). The superconducting gap is determined from the distance between the pair of dashed lines in panels (d) and (e). a.u.: arbitrary units.

Sr₂RuO₄ [46, 47]. In contrast, as illustrated by the dashed lines in Fig. 4(e), on the strained sample, we find a much larger value for $2\Delta_0$ of approximately 1.2 mV . We note that the gap measured by STM is likely to be dominated by the α and β sheets. As discussed in Ref. [46], the α and β sheets are dominated by xz and yz orbital weight and the tunneling conductance is likely to be much higher for the xz and yz orbitals than the xy orbital due to their greater extent along the z

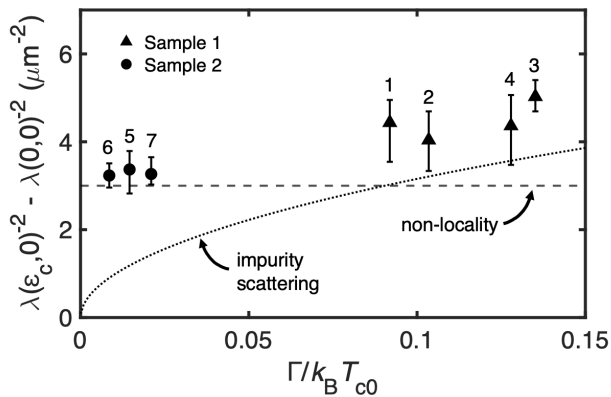


FIG. 5. Superfluid density enhancement at ϵ_c plotted against the scattering rate Γ determined from the unstrained T_c as described in the text and normalized by $k_B T_{c0}$. The labels at each marker correspond to the location on the samples indicated in Fig. 2(a) and (b). Point 7 was measured outside the scan range of Fig. 2(b). The error bars indicate the range of values observed over several measurement cycles and the data points represent the average value. The dotted line shows the prediction from reduced sensitivity to impurities, and the dashed line from reduced non-locality, both under an assumption that Δ_0 increases in proportion to T_c .

axis.

Importantly for discussion of the superfluid density, the gap on the α and β sheets is well away from the Van Hove point in k -space (points labeled Y in Fig. 1); due to the low Fermi velocity, carriers near the Van Hove point will not contribute strongly to the superfluid density. We therefore restrict our analysis of the superfluid density results to regions of the Fermi surface away from the Van Hove point. An enhanced m^* should increase $\lambda(0)$, thereby reducing the superfluid density. In contrast, our results show an increase in superfluid density, suggesting that any enhancement in m^* near the Lifshitz transition is too small to have a dominant effect. Angle-resolved photoemission spectroscopy (ARPES) data show that there is no substantial change in band renormalization as the γ sheet is tuned to the Lifshitz transition by substitution [48], and ARPES data under uniaxial stress show, similarly, no dramatic change [23]. Therefore, we suppose that m^* on sections of the Fermi surface away from the Van Hove point remains approximately constant as stress is applied.

We suppose further that away from the Van Hove point, the gap increases in proportion to T_c (the gap is likely substantial at the Van Hove point [49], but the superfluid density is not sensitive to this due to the low Fermi velocity). For a nodal superconductor, an enhanced gap can lead to an increased superfluid density in two ways: (1) reduced sensitivity to impurity scattering and (2) reduced non-local effects in the Meissner screening. For the case of impurities in a d -wave superconductor [16], it was shown that $\lambda(0)$ increases from its value in the clean, local limit λ_0 by an amount that depends on the magnitude of the superconducting gap: $\lambda(0) - \lambda_0 \sim \lambda_0 \sqrt{\Gamma/\Delta_0}$, where Γ is the nonmagnetic impurity scattering rate. Studies of T_c on samples with varying levels of impurities [50–53] show a suppression of T_c with increas-

ing impurity concentration that follows an Abrikosov-Gorkov (AG) relation, $\ln(T_{c0}/T_c) = \psi(1/2 + \Gamma/2\pi k_B T_c) - \psi(1/2)$ [54, 55], where ψ is the digamma function and T_{c0} is the clean-limit T_c . Therefore, taking T_c as a measure of Γ , we would expect a greater enhancement of the superfluid density at the Lifshitz transition for samples that have lower unstrained T_c .

In Fig. 5, we show the increase in superfluid density at ϵ_c for each point measured on the samples (see Fig. 2) plotted against $\Gamma/k_B T_{c0}$, where Γ is determined from the AG relation applied to $T_c(\epsilon = 0)$. Measurements on sample 1, which has lower $T_c(\epsilon = 0)$, indeed show a larger increase in superfluid density at the Lifshitz transition. However, the trend of the data does not match the expectation from impurity effects alone: the increase in superfluid density in sample 2 remains large, even though its $T_c(\epsilon = 0)$ is very close to the clean-limit value.

At sufficiently low temperature, non-local effects in the Meissner screening are expected to become important in all nodal superconductors because the coherence length, defined as $\xi(k) = \hbar v_F(k)/\pi\Delta(k)$, diverges along the nodal directions such that $\xi(k) > \lambda_0$ is satisfied near the nodes [21]. Similar to the effect of impurities, the low-temperature behaviour of $\lambda(T)$ becomes quadratic and $\lambda(0)$ increases from λ_0 . In a d -wave superconductor [21], the correction to $\lambda(0)$ can be estimated as $\lambda(0) - \lambda_0 = \lambda_0 \pi \sqrt{2}/16\kappa$. Taking $\lambda_0 = 190$ nm and a zero-temperature coherence length of $\xi_0 = 66$ nm [2], the non-local correction to $\lambda(0)$ is approximately 10% of λ_0 in unstrained Sr_2RuO_4 . T_c increases by a factor of 2.3 between $\epsilon = 0$ and the Lifshitz transition. If we take κ to increase by this same factor, we find that $\lambda(0)$ decreases by ≈ 10 nm; $\lambda(0)^{-2}$ increases by $\approx 3 \mu\text{m}^{-2}$. This increase is shown by the dashed line in Fig. 5 and is consistent with the superfluid enhancement observed on sample 2. We note that the twenty-fold increase in H_{c2} [22, 25] indicates a greater decrease in ξ_0 by a factor of $\sqrt{20}$. However, the highly anisotropic electronic structure of Sr_2RuO_4 tuned to the Lifshitz transition should be recalled: this increase in H_{c2} could be driven by carriers in the immediate vicinity of the Van Hove point. The value of the penetration depth measurements is that they provide information on how portions of the Fermi surface away from the Van Hove point, where the Fermi velocity is larger, respond to the tuning to the Lifshitz transition.

In summary, the zero-temperature superfluid density in Sr_2RuO_4 undergoes a $\sim 15\%$ enhancement as the system is strain-tuned through the VHS, and the penetration depth shows a $\lambda(T) \sim T^2$ dependence throughout the Lifshitz transition. In addition, the superconducting gap increases with strain going from $\Delta_0 \approx 350 \mu\text{eV}$ in an unstrained sample to $\Delta_0 \approx 600 \mu\text{eV}$ in a sample strained to near the Lifshitz transition. Our analysis indicates that the increase in superfluid density with tuning to the Lifshitz transition is primarily driven by a decrease in non-local effects in the Meissner screening. We note that Ref. [56] reports measurements of H_{c1} in unstrained Sr_2RuO_4 that also highlight the importance of non-local effects. Both the STM and the penetration depth measurements, which are sensitive primarily to regions of Fermi surface away from the Van Hove point, show that tuning to the Lifshitz tran-

sition increases the gap throughout the Brillouin zone, an observation that might be a useful clue on the pairing mechanism in Sr_2RuO_4 .

This work was supported by the Department of Energy, Office of Basic Energy Sciences, Division of Materials Sciences and Engineering, under contract DE-AC02-76SF00515. N. K. is supported by JSPS KAKENHI (No. JP18K04715, No. JP21H01033, and No. JP22K19093). YM was supported by JSPS KAKENHI (Nos. JP15H05851 and JP22H01168). GSO was supported by JSPS KAKENHI (Nos. JP15H05851, JP15K21717) during his stay at Kyoto University. We thank Gwansuk Oh for his contribution to the crystal growth. F.J., A.P.M. and C.W.H. acknowledge the support of the Max Planck Society and the German Research

Foundation (TRR288-422213477 ELASTO-Q-MAT, Project A10). Research in Dresden benefits from the environment provided by the DFG Cluster of Excellence (ct.qmat EXC 2147, Project 390858490. C.W.H. acknowledges support from the Engineering and Physical Sciences Research Council (U.K.) (EP/X01245X/1). This work was supported by the Center for Quantum Sensing and Quantum Materials, an Energy Frontier Research Center funded by the U. S. Department of Energy, Office of Science, Basic Energy Sciences under Award DE-SC0021238. We acknowledge useful conversations with J. Landaeta and E. Hassinger.

-
- [1] Y. Maeno, H. Hashimoto, K. Yoshida, S. Nishizaki, T. Fujita, J. Bednorz, and F. Lichtenberg, Superconductivity in a layered perovskite without copper, *Nature* **372**, 532 (1994).
- [2] A. P. Mackenzie and Y. Maeno, The superconductivity of Sr_2RuO_4 and the physics of spin-triplet pairing, *Rev. Mod. Phys.* **75**, 657 (2003).
- [3] A. P. Mackenzie, A personal perspective on the unconventional superconductivity of Sr_2RuO_4 , *J. Supercond. Novel Mag.* **33**, 177 (2020).
- [4] A. P. Mackenzie, T. Scaffidi, C. W. Hicks, and Y. Maeno, Even odder after twenty-three years: the superconducting order parameter puzzle of Sr_2RuO_4 , *npj Quantum Mater.* **2**, 1 (2017).
- [5] Y. Maeno, S. Kittaka, T. Nomura, S. Yonezawa, and K. Ishida, Evaluation of spin-triplet superconductivity in Sr_2RuO_4 , *J. Phys. Soc. Jpn.* **81**, 011009 (2011).
- [6] C. Kallin, Chiral p-wave order in Sr_2RuO_4 , *Rep. Prog. Phys.* **75**, 042501 (2012).
- [7] Y. Liu and Z.-Q. Mao, Unconventional superconductivity in Sr_2RuO_4 , *Physica C* **514**, 339 (2015).
- [8] A. J. Leggett and Y. Liu, Symmetry properties of superconducting order parameter in Sr_2RuO_4 , *J. Supercond. Novel Mag.* **34**, 1647 (2021).
- [9] C. Bergemann, A. P. Mackenzie, S. Julian, D. Forsythe, and E. Ohmichi, Quasi-two-dimensional Fermi liquid properties of the unconventional superconductor Sr_2RuO_4 , *Advances in Physics* **52**, 639 (2003).
- [10] S. Nishizaki, Y. Maeno, and Z. Mao, Changes in the superconducting state of Sr_2RuO_4 under magnetic fields probed by specific heat, *J. Phys. Soc. Jpn.* **69**, 572 (2000).
- [11] K. Deguchi, Z. Mao, H. Yaguchi, and Y. Maeno, Gap structure of the spin-triplet superconductor Sr_2RuO_4 determined from the field-orientation dependence of the specific heat, *Phys. Rev. Lett.* **92**, 047002 (2004).
- [12] S. Kittaka, S. Nakamura, T. Sakakibara, N. Kikugawa, T. Terashima, S. Uji, D. A. Sokolov, A. P. Mackenzie, K. Irie, Y. Tsutsumi, *et al.*, Searching for gap zeros in Sr_2RuO_4 via field-angle-dependent specific-heat measurement, *J. Phys. Soc. Jpn.* **87**, 093703 (2018).
- [13] K. Izawa, H. Takahashi, H. Yamaguchi, Y. Matsuda, M. Suzuki, T. Sasaki, T. Fukase, Y. Yoshida, R. Settai, and Y. Onuki, Superconducting gap structure of spin-triplet superconductor Sr_2RuO_4 studied by thermal conductivity, *Phys. Rev. Lett.* **86**, 2653 (2001).
- [14] M. Suzuki, M. Tanatar, N. Kikugawa, Z. Mao, Y. Maeno, and T. Ishiguro, Universal heat transport in Sr_2RuO_4 , *Phys. Rev. Lett.* **88**, 227004 (2002).
- [15] E. Hassinger, P. Bourgeois-Hope, H. Taniguchi, S. R. de Cotret, G. Grissonnanche, M. S. Anwar, Y. Maeno, N. Doiron-Leyraud, and L. Taillefer, Vertical line nodes in the superconducting gap structure of Sr_2RuO_4 , *Phys. Rev. X* **7**, 011032 (2017).
- [16] P. J. Hirschfeld and N. Goldenfeld, Effect of strong scattering on the low-temperature penetration depth of a d-wave superconductor, *Phys. Rev. B* **48**, 4219 (1993).
- [17] I. Bonalde, B. D. Yanoff, M. Salamon, D. Van Harlingen, E. Chia, Z. Mao, and Y. Maeno, Temperature dependence of the penetration depth in Sr_2RuO_4 : evidence for nodes in the gap function, *Phys. Rev. Lett.* **85**, 4775 (2000).
- [18] R. Ormeno, M. Hein, T. Barraclough, A. Sibley, C. Gough, Z. Mao, S. Nishizaki, and Y. Maeno, Electrodynamic response of Sr_2RuO_4 , *Phys. Rev. B* **74**, 092504 (2006).
- [19] P. Baker, R. Ormeno, C. Gough, Z. Mao, S. Nishizaki, and Y. Maeno, Microwave surface impedance measurements of Sr_2RuO_4 : The effect of impurities, *Phys. Rev. B* **80**, 115126 (2009).
- [20] Z. Mao, Y. Maeno, and H. Fukazawa, Crystal growth of Sr_2RuO_4 , *Materials Research Bulletin* **35**, 1813 (2000).
- [21] I. Kosztin and A. J. Leggett, Nonlocal effects on the magnetic penetration depth in d-wave superconductors, *Phys. Rev. Lett.* **79**, 135 (1997).
- [22] A. Steppke, L. Zhao, M. E. Barber, T. Scaffidi, F. Jerzembeck, H. Rosner, A. S. Gibbs, Y. Maeno, S. H. Simon, A. P. Mackenzie, and C. W. Hicks, Strong peak in T_c of Sr_2RuO_4 under uniaxial pressure, *Science* **355**, eaaf9398 (2017).
- [23] V. Sunko, E. Abarca Morales, I. Marković, M. E. Barber, D. Milosavljević, F. Mazzola, D. A. Sokolov, N. Kikugawa, C. Cacho, P. Dudin, *et al.*, Direct observation of a uniaxial stress-driven Lifshitz transition in Sr_2RuO_4 , *npj Quantum Mater.* **4**, 46 (2019).
- [24] C. W. Hicks, D. O. Brodsky, E. A. Yelland, A. S. Gibbs, J. A. N. Bruin, M. E. Barber, S. D. Edkins, K. Nishimura, S. Yonezawa, Y. Maeno, A. P. Mackenzie, B. Baghi, C. W. Hicks, D. Brodsky, and A. Edward, Strong increase of T_c of Sr_2RuO_4 under both tensile and compressive strain, *Science* **344**, 283 (2014).
- [25] F. Jerzembeck, A. Steppke, A. Pustogow, Y. Luo, A. Chronister, D. A. Sokolov, N. Kikugawa, Y.-S. Li, M. Nicklas, S. E. Brown, *et al.*, Upper critical field of Sr_2RuO_4 under in-plane uniaxial pressure, *Phys. Rev. B* **107**, 064509 (2023).
- [26] Y.-T. Hsu, W. Cho, A. F. Rebola, B. Burganov, C. Adamo, K. M.

- Shen, D. G. Schlom, C. J. Fennie, and E.-A. Kim, Manipulating superconductivity in ruthenates through Fermi surface engineering, *Phys. Rev. B* **94**, 045118 (2016).
- [27] J. Mravlje, M. Aichhorn, T. Miyake, K. Haule, G. Kotliar, and A. Georges, Coherence-incoherence crossover and the mass-renormalization puzzles in Sr_2RuO_4 , *Phys. Rev. Lett.* **106**, 096401 (2011).
- [28] E. Mueller, Y. Iguchi, C. Watson, C. W. Hicks, Y. Maeno, and K. A. Moler, Constraints on a split superconducting transition under uniaxial strain in Sr_2RuO_4 from scanning squid microscopy, *Phys. Rev. B* **108**, 144501 (2023).
- [29] V. Grinenko, S. Ghosh, R. Sarkar, J. C. Orain, A. Nikitin, M. Elender, D. Das, Z. Guguchia, F. Brückner, M. E. Barber, J. Park, N. Kikugawa, D. A. Sokolov, J. S. Bobowski, T. Miyoshi, Y. Maeno, A. P. Mackenzie, H. Luetkens, C. W. Hicks, and H. H. Klauss, Split superconducting and time-reversal symmetry-breaking transitions in Sr_2RuO_4 under stress, *Nat. Phys.* **17**, 748 (2021).
- [30] J. R. Kirtley, L. Paulius, A. J. Rosenberg, J. C. Palmstrom, C. M. Holland, E. M. Spanton, D. Schiessl, C. L. Jermain, J. Gibbons, Y. K. Fung, M. E. Huber, D. C. Ralph, M. B. Ketchen, G. W. Gibson, and K. A. Moler, Scanning SQUID susceptometers with sub-micron spatial resolution, *Rev. Sci. Instrum.* **87**, 093702 (2016).
- [31] J. R. Kirtley, B. Kalisky, J. A. Bert, C. Bell, M. Kim, Y. Hikita, H. Y. Hwang, J. H. Ngai, Y. Segal, F. J. Walker, C. H. Ahn, and K. A. Moler, Scanning SQUID susceptometry of a paramagnetic superconductor, *Phys. Rev. B* **85**, 224518 (2012).
- [32] C. W. Hicks, M. E. Barber, S. D. Edkins, D. O. Brodsky, and A. P. Mackenzie, Piezoelectric-based apparatus for strain tuning, *Rev. Sci. Instrum.* **85**, 065003 (2014).
- [33] C. A. Watson, A. S. Gibbs, A. P. Mackenzie, C. W. Hicks, and K. A. Moler, Micron-scale measurements of low anisotropic strain response of local T_c in Sr_2RuO_4 , *Phys. Rev. B* **98**, 094521 (2018).
- [34] M. E. Barber, F. Lechermann, S. V. Streltsov, S. L. Skornyakov, S. Ghosh, B. Ramshaw, N. Kikugawa, D. A. Sokolov, A. P. Mackenzie, C. W. Hicks, *et al.*, Role of correlations in determining the Van Hove strain in Sr_2RuO_4 , *Phys. Rev. B* **100**, 245139 (2019).
- [35] See Supplemental Material at [URL will be inserted by publisher].
- [36] S. Nishizaki, Y. Maeno, and T. Fujita, Effect of annealing on the superconductivity of Sr_2RuO_4 , *J. Phys. Soc. Jpn.* **65**, 1876 (1996).
- [37] T_c has been shown to be relatively stable to changes in oxygen partial pressure annealing conditions [36]. Therefore, the stripe features in local T_c most likely correspond to ruthenium deficiencies that periodically accumulate during sample growth.
- [38] C. A. Marques, L. C. Rhodes, R. Fittipaldi, V. Granata, C. M. Yim, R. Buzio, A. Gerbi, A. Vecchione, A. W. Rost, and P. Wahl, Magnetic-field tunable intertwined checkerboard charge order and nematicity in the surface layer of Sr_2RuO_4 , *Advanced Materials* **33**, 2100593 (2021).
- [39] Z. Wang, D. Walkup, P. Derry, T. Scaffidi, M. Rak, S. Vig, A. Kogar, I. Zeljkovic, A. Husain, L. H. Santos, *et al.*, Quasi-particle interference and strong electron-mode coupling in the quasi-one-dimensional bands of Sr_2RuO_4 , *Nat. Phys.* **13**, 799 (2017).
- [40] H. Kambara, Y. Niimi, K. Takizawa, H. Yaguchi, Y. Maeno, and H. Fukuyama, Scanning tunneling microscopy and spectroscopy of Sr_2RuO_4 , in *AIP Conf. Proc.*, Vol. 850 (2006) pp. 539–540.
- [41] B. Barker, S. Dutta, C. Lupien, P. McEuen, N. Kikugawa, Y. Maeno, and J. Davis, STM studies of individual Ti impurity atoms in Sr_2RuO_4 , *Physica B: Condensed Matter* **329**, 1334 (2003).
- [42] A. Kreisel, C. Marques, L. Rhodes, X. Kong, T. Berlijn, R. Fittipaldi, V. Granata, A. Vecchione, P. Wahl, and P. Hirschfeld, Quasi-particle interference of the van hove singularity in Sr_2RuO_4 , *npj Quantum Mater.* **6**, 100 (2021).
- [43] R. Matzdorf, Z. Fang, Ismail, J. Zhang, T. Kimura, Y. Tokura, K. Terakura, and E. Plummer, Ferromagnetism stabilized by lattice distortion at the surface of the p-wave superconductor Sr_2RuO_4 , *Science* **289**, 746 (2000).
- [44] C. N. Veenstra, Z.-H. Zhu, B. Ludbrook, M. Capsoni, G. Levy, A. Nicolaou, J. A. Rosen, R. Comin, S. Kittaka, Y. Maeno, I. S. Elfimov, and A. Damascelli, Determining the surface-to-bulk progression in the normal-state electronic structure of Sr_2RuO_4 by angle-resolved photoemission and density functional theory, *Phys. Rev. Lett.* **110**, 097004 (2013).
- [45] E. Abarca Morales, G.-R. Siemann, A. Zivanovic, P. A. E. Murgatroyd, I. Marković, B. Edwards, C. A. Hooley, D. A. Sokolov, N. Kikugawa, C. Cacho, M. D. Watson, T. K. Kim, C. W. Hicks, A. P. Mackenzie, and P. D. C. King, Hierarchy of lifshitz transitions in the surface electronic structure of sr_2ruo_4 under uniaxial compression, *Phys. Rev. Lett.* **130**, 096401 (2023).
- [46] I. Firmo, S. Lederer, C. Lupien, A. P. Mackenzie, J. Davis, and S. Kivelson, Evidence from tunneling spectroscopy for a quasi-one-dimensional origin of superconductivity in Sr_2RuO_4 , *Phys. Rev. B* **88**, 134521 (2013).
- [47] R. Sharma, S. D. Edkins, Z. Wang, A. Kostin, C. Sow, Y. Maeno, A. P. Mackenzie, J. S. Davis, and V. Madhavan, Momentum-resolved superconducting energy gaps of Sr_2RuO_4 from quasiparticle interference imaging, *Proceedings of the National Academy of Sciences* **117**, 5222 (2020).
- [48] K. Shen, N. Kikugawa, C. Bergemann, L. Balicas, F. Baumberger, W. Meevasana, N. Ingle, Y. Maeno, Z.-X. Shen, and A. P. Mackenzie, Evolution of the Fermi surface and quasiparticle renormalization through a van Hove singularity in $\text{Sr}_{2-y}\text{La}_y\text{RuO}_4$, *Phys. Rev. Lett.* **99**, 187001 (2007).
- [49] Y.-S. Li, M. Garst, J. Schmalian, S. Ghosh, N. Kikugawa, D. A. Sokolov, C. W. Hicks, F. Jerzembeck, M. S. Ikeda, Z. Hu, B. J. Ramshaw, A. W. Rost, M. Nicklas, and A. P. Mackenzie, Elastocaloric determination of the phase diagram of Sr_2RuO_4 , *Nature* **607**, 276 (2022).
- [50] A. P. Mackenzie, R. Haselwimmer, A. Tyler, G. Lonzarich, Y. Mori, S. Nishizaki, and Y. Maeno, Extremely strong dependence of superconductivity on disorder in Sr_2RuO_4 , *Phys. Rev. Lett.* **80**, 161 (1998).
- [51] Z. Mao, Y. Mori, and Y. Maeno, Suppression of superconductivity in Sr_2RuO_4 caused by defects, *Phys. Rev. B* **60**, 610 (1999).
- [52] N. Kikugawa and Y. Maeno, Non-Fermi-liquid behavior in Sr_2RuO_4 with nonmagnetic impurities, *Phys. Rev. Lett.* **89**, 117001 (2002).
- [53] N. Kikugawa, A. P. Mackenzie, C. Bergemann, R. Borzi, S. Grigera, and Y. Maeno, Rigid-band shift of the Fermi level in the strongly correlated metal: $\text{Sr}_{2-y}\text{La}_y\text{RuO}_4$, *Phys. Rev. B* **70**, 060508 (2004).
- [54] A. A. Abrikosov and L. P. Gor'kov, Contribution to the theory of superconducting alloys with paramagnetic impurities, *Zhur. Eksptl'. i Teoret. Fiz.* **39** (1960).
- [55] P. Hirschfeld, P. Wölfle, and D. Einzel, Consequences of resonant impurity scattering in anisotropic superconductors: Thermal and spin relaxation properties, *Phys. Rev. B* **37**, 83 (1988).
- [56] J. F. Landaeta, K. Semeniuk, J. Aretz, K. Shirer, D. A. Sokolov, N. Kikugawa, Y. Maeno, I. Bonalde, J. Schmalian, A. P. Mackenzie, and E. Hassinger, Evidence for vertical line nodes

in Sr_2RuO_4 from nonlocal electrodynamics, arXiv preprint

arXiv:2312.05129 (2023).

Supplementary Materials for: Superconducting Penetration Depth Through a Van Hove Singularity: Sr_2RuO_4 Under Uniaxial Stress

Eli Mueller,^{1,2} Yusuke Iguchi,^{1,3} Fabian Jerzembeck,⁴ Jorge O. Rodriguez,⁵ Marisa Romanelli,⁵ Edgar Abarca-Morales,⁴ Anastasios Markou,^{4,6} Naoki Kikugawa,⁷ Dmitry A. Sokolov,⁴ Gwansuk Oh,^{8,9} Clifford W. Hicks,^{4,10} Andrew P. Mackenzie,^{4,11} Yoshiteru Maeno,^{8,12} Vidya Madhavan,⁵ and Kathryn A. Moler^{1,2,3}

¹Stanford Institute for Materials and Energy Sciences, SLAC National Accelerator Laboratory, 2575 Sand Hill Road, Menlo Park, California 94025, USA

²Department of Physics, Stanford University, Stanford, California 94305, USA

³Geballe Laboratory for Advanced Materials, Stanford University, Stanford, California 94305, USA

⁴Max Planck Institute for the Chemical Physics of Solids, Nöthnitzer Straße 40, Dresden 01187, Germany

⁵Department of Physics, University of Illinois, Urbana, Illinois 61801, USA

⁶Department of Physics, University of Ioannina, 45110 Ioannina, Greece

⁷National Institute for Materials Science, Tsukuba, Ibaraki 305-0003, Japan

⁸Department of Physics, Graduate School of Science, Kyoto University, Kyoto 606-8502, Japan

⁹Department of Physics, Pohang University of Science and Technology (POSTECH), Pohang 790-784, Republic of Korea

¹⁰School of Physics and Astronomy, University of Birmingham, Birmingham B15 2TT, United Kingdom

¹¹Scottish Universities Physics Alliance, School of Physics and Astronomy, University of St. Andrews, St. Andrews KY16 9SS, United Kingdom

¹²Toyota Riken - Kyoto University Research Center (TRiKUC), Kyoto University, Kyoto 606-8501, Japan

I. ADDITIONAL INFORMATION: STM

Uniaxial strain was applied in the STM measurement using a thermal expansion cell described in Ref. [1] and adapted from that used in Ref. [2]. The STM strain cell was calibrated using digital image correlation (DIC) and elastoresistivity measurements described in Ref. [1] which estimated the strain of the sample platform to be approximately -0.47% to -0.5%. The surface of the sample is under less strain than the sample platform itself and based on profilometry measurements of the sample thickness after cleaving, we estimate the strain at the sample surface to be approximately -0.4%.

We determined the topographical depths of the cleavage defects by flattening the three dimensional topographic dataset into two dimensions, via $T(x,y) \rightarrow T(x)$, along the vertical dimension. The topographic values on this restructured array are then binned by frequency for a particular value of x . The lower panel of Fig. S1(b) shows this projected and binned data, while the upper panel shows the original topography. From this analysis, we see that the difference in height between the upper and lower surfaces is approximately 3.4 Å, in good agreement with the established value of 3.8 Å for the separation between two SrO layers and much larger than the 2.1 Å separation between SrO and RuO₂ layers, as illustrated in the schematic of the defect in Fig. S1(a).

II. ADDITIONAL INFORMATION: SCANNING SQUID

The local T_c maps shown in Fig. 2 of the main text were made by taking spatial scans of M at various temperatures near the unstressed bulk T_c of the sample and at the base temperature $T_{\text{base}} \approx 500$ mK with a fixed scan height. At each temperature, the maps of $M(T)$ are converted to maps of $\lambda(T) + z_0$. We assume constant z_0 for all scans so that temperature dependent changes in $\lambda(T) + z_0$ correspond to changes in $\lambda(T)$. For each pixel in the temperature series scans, we set $\Delta\lambda(T) = \lambda(T) - \lambda(T_{\text{base}})$ and we calculated the normalized superfluid density $\rho(T) = \lambda_0^2 / (\lambda_0 + \Delta\lambda(T))^2$ using $\lambda_0 = 190$ nm. We performed a T -linear fit of $\rho(T)$ near the bulk T_c and set the local T_c to be the temperature of the $\rho = 0$ intercept. We note that the calculation of $\rho(T)$ here assumes a constant and spatially uniform penetration depth of $\lambda_0 = 190$ nm for $0 < T < T_{\text{base}}$; however, varying λ_0 by ± 20 nm does not substantially change the values of $\rho(T)$ very close to the bulk T_c and therefore does not significantly change the resulting local T_c map.

Data on the strain- and temperature-dependent changes of the penetration depth shown in Fig. 3(a) and (b) of the main text were obtained by bringing the SQUID susceptometer into mechanical contact with a selected point on the sample and recording M while sweeping the temperature from $T_{\text{base}} \approx 500$ mK to above T_c for a series of applied strains. Figure S2 shows the temperature dependence of the mutual inductance $M(T)$ measured under a series of compressive strains through the Lifshitz transition on sample 1 [Fig. S2(a) and (b)] and sample 2 [Fig. S2(c) and (d)]. We observed rounding of the superconducting transition under increasing strain due to strain inhomogeneity within the measurement volume. The local T_c at each strain is defined by the temperature at which dM/dT was maximal and is indicated by the red data points in S2.

The main text shows data on the temperature and strain dependence of the change in penetration depth $\lambda(\varepsilon, T) - \lambda(0, 0)$ measured on sample 2. The data measured on sample 1 are shown in Fig. S3. Consistent with measurements on sample 2, the penetration depth shows a $\sim T^2$ dependence for $T < 0.5T_c$ throughout the Lifshitz transition.

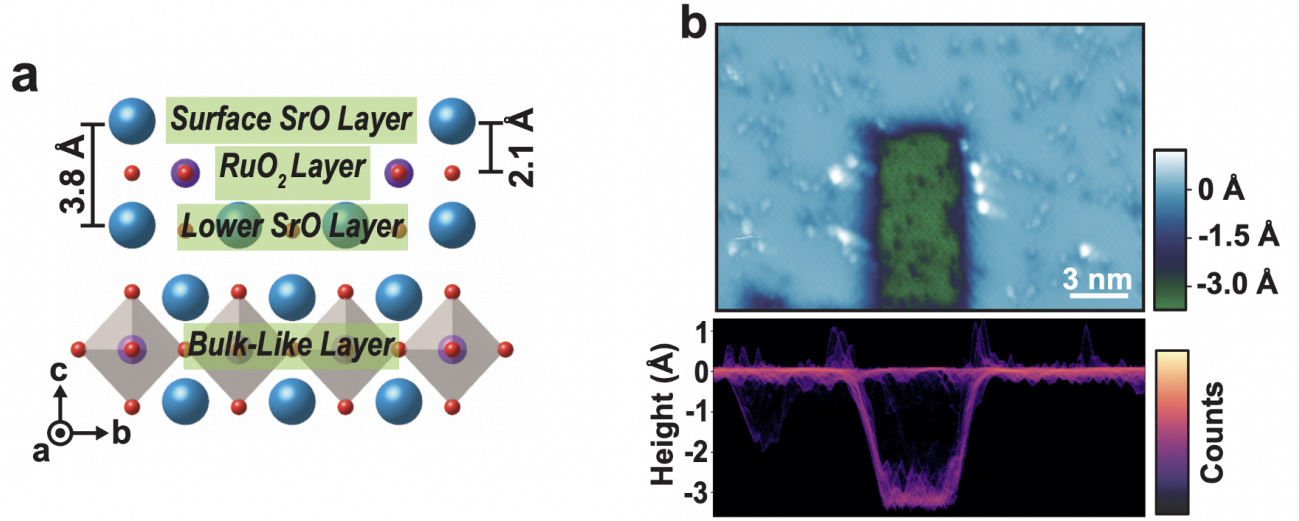


FIG. S1. (a) Schematic diagram of the large crystallographic defects on the surface of strontium ruthenate. We identify two different types, which expose a different crystal layer, SrO and RuO₂. (b) Topographic image (upper panel) of a defect on the surface of strontium ruthenate. The density histogram (lower panel) of the topographic image shown, projected along y and binned, allows us to better visualize the mean depth of 3.4 Å

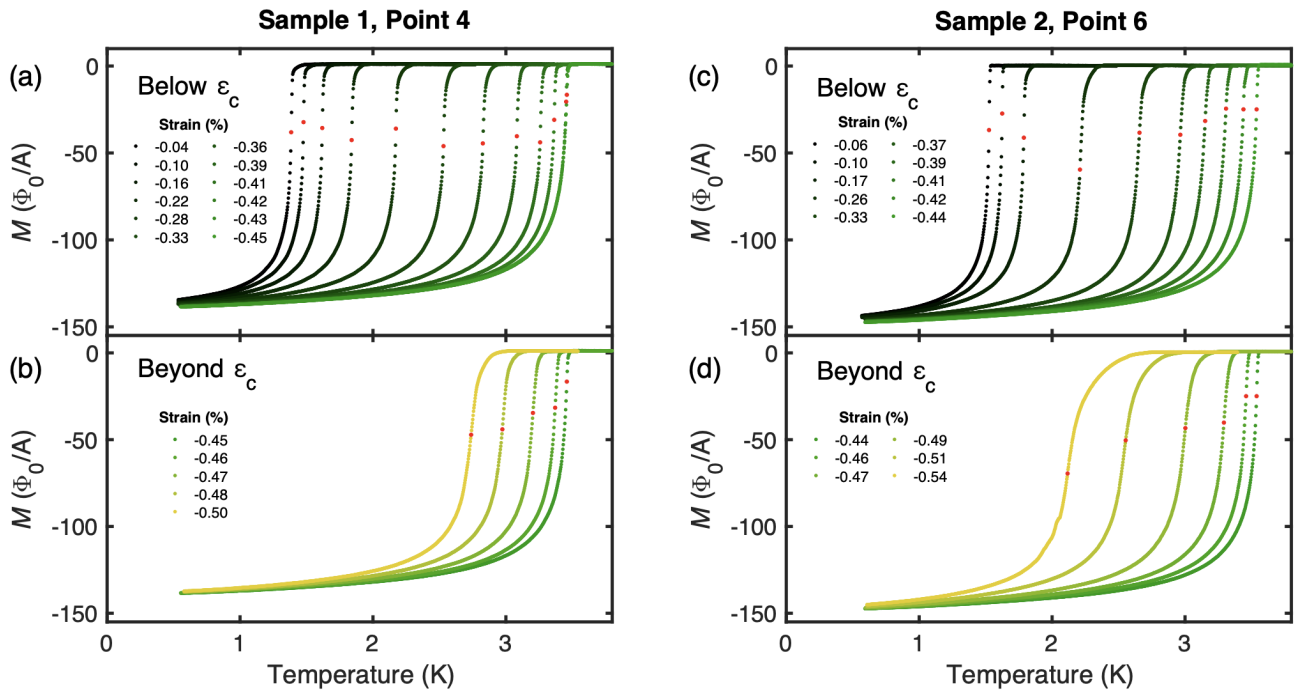


FIG. S2. (a) and (b) $M(T)$ measured on sample 1 for strains below ε_c and above ε_c respectively. (c) and (d) $M(T)$ measured on sample 2 for strains below ε_c and above ε_c respectively. Red data points indicate where the slope of $M(T)$ is maximal and the temperature at which we take to be the local T_c

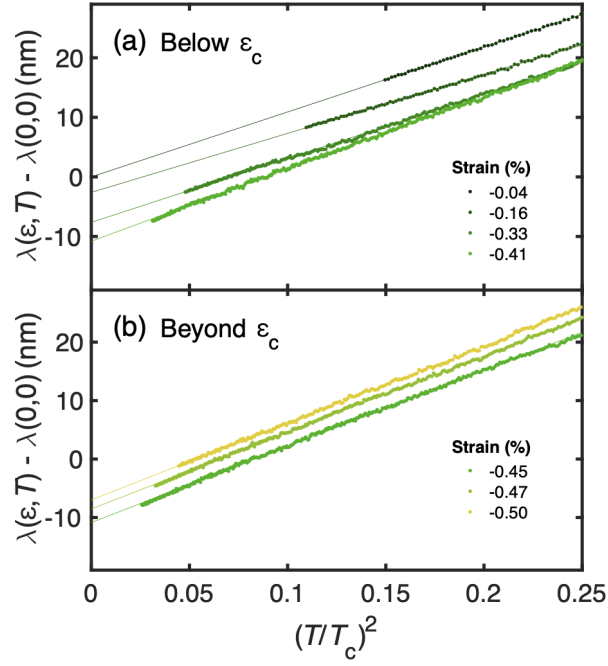


FIG. S3. Temperature and strain dependence of the penetration depth measured at point 4 on sample 1. Panels (a) and (b) correspond to strain values below and above ϵ_c respectively.

-
- [1] J. Olivares Rodriguez, *Stress and crystal imperfections: Tools for the exploration of unconventional superconductivity via scanning tunneling microscopy*, Ph.D. thesis, University of Illinois Urbana-Champaign (2022).
- [2] V. Sunko, E. Abarca Morales, I. Marković, M. E. Barber, D. Milosavljević, F. Mazzola, D. A. Sokolov, N. Kikugawa, C. Cacho, P. Dudin, *et al.*, Direct observation of a uniaxial stress-driven Lifshitz transition in Sr_2RuO_4 , *npj Quantum Mater.* **4**, 46 (2019).